

Self-diffusion is temperature independent on active membranes

Saurav G. Varma,^{*} Argha Mitra,[†] and Sumantra Sarkar[‡]

Center for Condensed Matter Theory, Department of Physics,

Indian Institute of Science, Bengaluru, Karnataka, 560012

(Dated: April 17, 2024)

arXiv:2404.10581v1 [cond-mat.soft] 16 Apr 2024

Abstract

Molecular transport maintains cellular structures and functions. For example, lipid and protein diffusion sculpts the dynamic shapes and structures on the cell membrane that perform essential cellular functions, such as cell signaling. Temperature variations in thermal equilibrium rapidly change molecular transport properties. The coefficient of lipid self-diffusion increases exponentially with temperature in thermal equilibrium, for example. Hence, in the noisy cellular environment, where temperatures can fluctuate widely due to local heat generation, maintaining cellular homeostasis through molecular transport is hard in thermal equilibrium. In this paper, using both molecular and lattice-based modeling of membrane transport, we show that the presence of active transport originating from the cell's cytoskeleton can make the self-diffusion of the molecules on the membrane robust to temperature fluctuations. The resultant temperature-independence of self-diffusion keeps the precision of cellular signaling invariant over a broad range of ambient temperatures, allowing cells to make robust decisions. We have also found that the Kawasaki algorithm, the widely used model of lipid transport on lattices, predicts incorrect temperature dependence of lipid self-diffusion in equilibrium. We propose a new algorithm that correctly captures the equilibrium properties of lipid self-diffusion and reproduces experimental observations.

I. INTRODUCTION

Molecular transport is essential for various physical and biological processes. In cells, where molecules are the primary drivers of all structure and function, spatial organization and transport of molecules determine the robustness and accuracy of various cellular processes. For example, diffusion, one of the primary modes of transport for cellular molecules, imposes a fundamental limit on the cell's ability to sense its environment [1]. Hence, understanding the factors that govern the molecular transport processes in cells, such as molecular crowding [2, 3] or interaction with the actin cytoskeleton (ACS) [4–7], is of general interest. In this paper, we investigate the effect of the ACS on lipid transport on the plasma membrane and show that the nonequilibrium (active) forces imparted by ACS on the lipids fundamentally change the nature of molecular transport on the plasma membrane (PM).

* sauravvarma@iisc.ac.in

† arghamitra@iisc.ac.in

‡ sumantra@iisc.ac.in

Cellular transport primarily happens through two mechanisms: diffusion, which obeys the detailed balance principle, and active transport, which breaks detailed balance [8]. The constraint of detailed balance is a defining feature of an equilibrium system. It states that the probability flux from a state i to a state j exactly equals the flux from state j to state i . Mathematically,

$$p_i \pi_{ij} = p_j \pi_{ji}, \quad (1)$$

where $p_{i(j)}$ is the occupation probability of state $i(j)$ and π_{ij} is the transition probability from state i to state j . In cells, active transport is facilitated by motor proteins, which consume ATP to drive various cellular structures out of equilibrium. For example, they interact with the cortical ACS, a meshwork of actin filaments adjoining the cell's PM, and make them active. The interaction of the active ACS with the PM leads to patterns, structures, and behaviors that are not found in thermal equilibrium [9–11]. These changes are brought in by the active transport of various molecules on the plasma membrane (PM) [12], whose repercussions are often significantly different from its passive counterpart [13].

As a concrete example, let's consider the diffusion coefficient's temperature (T)-dependence. Diffusion of a free colloid obeys the Stokes-Einstein relationship, which states that $D(T) = k_B T / \gamma$, where k_B is the Boltzmann constant and γ is the friction coefficient. Also, the diffusion of molecules adsorbed on periodic surfaces is determined by escape from the periodic potential generated by the surface molecules, which results in an Arrhenius-like form for the diffusion coefficient:

$$D(T) = D_0 e^{-\frac{E_A}{k_B T}}, \quad (2)$$

where E_A is proportional to the surface potential [14]. Self-diffusion of molecules also follows the Arrhenius kinetics, where the many-body interaction between the molecules determines the E_A . Together, we will call them activated diffusion. Activated diffusion is often observed on model membranes, where E_A is of the order of tens of $k_B T$ [15–17]. In contrast, the T -dependence of diffusion is unclear on live cell plasma membrane, where active effects are predominant.

Recently, it was observed that, in live cells, Glycosylphosphatidylinositol anchored proteins (GPI-AP), a model cell surface protein and a known interaction partner of the ACS [13], shows T -independent diffusion [18]. This observation contradicts prior works, which show,

using very similar techniques (Fluorescence Correlation Spectroscopy: FCS), that diffusion is T -dependent even in live cells [17, 19–21]. Therefore, it remains unclear whether the transport of molecules in live cells is T -independent or not. An important observation is that the T -independence of diffusion is dependent on the scale of observation [18]. When the membrane is observed with a small FCS spot ($3 \times 10^4 \text{ nm}^2$), diffusion is T -independent. However, as the spot size increases ($6 \times 10^4 \text{ nm}^2$), diffusion becomes T -dependent [18]. Therefore, we hypothesize that processes that are important at the nanometer scale, such as the interaction of the membrane with the ACS, are the key drivers of T -independent transport of molecules. In this paper, we test this hypothesis using a coarse-grained molecular dynamic (CG-MD) model and a lattice model of model membranes.

Now, we briefly describe the results and the conclusions of the paper. The paper is broadly divided into two parts. In the first part, we ran equilibrium CG-MD simulations to study lipid self-diffusion in model membranes, which showed that diffusion is an activated process irrespective of the observation scale. In the second part of the paper, we tested the effect of an underlying nonequilibrium driving on the activated diffusion process. Specifically, we studied the effect of ACS on the lipid self-diffusion using a lattice model of lipids. We find that coupling to the ACS makes lipid diffusion T -independent. Surprisingly, lipids that do not couple to the ACS can also show near T -independence because of their interactions with the ACS-coupled lipids. We comment on the consequences of the T -independence and its biological relevance to end the paper. We have also found that the Kawasaki algorithm, which is used extensively to simulate lipid diffusion, does not accurately capture diffusion’s thermodynamics. We propose an alternate algorithm, called the barrier hop dynamics, which accurately captures the equilibrium kinetics of activated diffusion.

II. RESULTS

A. Bulk diffusivity in equilibrium is T -dependent

We first checked the behavior of the bulk transport coefficients of lipids as a function of temperature, T , using CG-MD simulation (see section A 1). We computed the lipids’ time and ensemble-averaged mean squared displacement (MSD) to measure the bulk transport coefficients (see A 2). The MSD curves showed clear T -dependence (Fig. 1a, S1, S2).

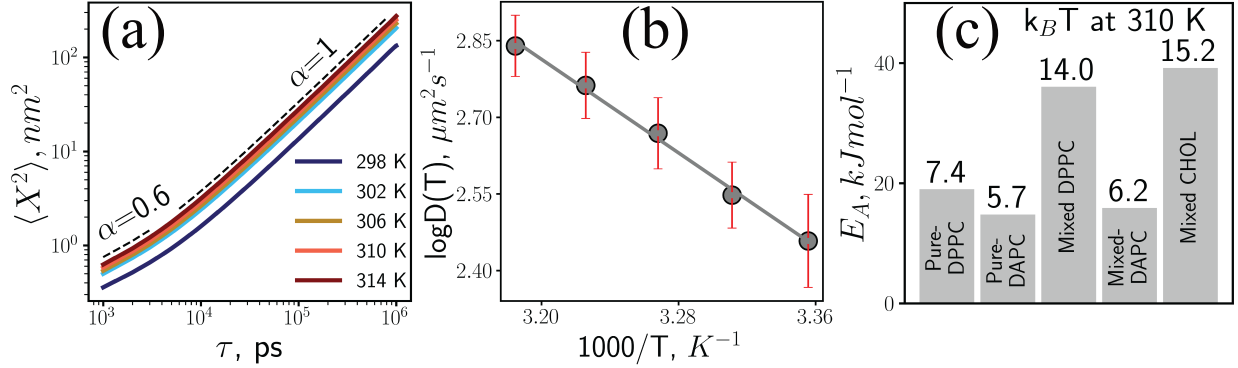


FIG. 1. Activated diffusion in CG-MD model. (a-b) MSD ($\langle X^2 \rangle$) and diffusivity (semilog scale) of pure DPPC membrane at different T (298 K - 314 K). (c) The activation energy (E_A) of lipids for different PM models $k_B T$ at 310 K. All the results from long time scale simulations. Error bars are the standard deviation of 8 replicates. In (b) $\log D(T)$ is plotted vs $1000/T$, as per experimental convention [17].

Also, all MSD curves had the characteristic subdiffusive regions for short lag time, τ , with an anomalous coefficient of 0.6 [22], and at long times, showed diffusive transport. We measured the diffusion coefficients at different temperatures, which varied according to the Arrhenius form (Eq: A2, A3 and Fig. 1b), as shown in various experiments before [23–26]. The activation energy, E_A ranges between 6 – 14 $k_B T$ (Fig 1c), which is in the same ballpark of experimental [17] and atomistic simulation data reported earlier [15, 27], which provides an independent check on the correctness of our simulations. Therefore, we conclude that, in equilibrium, lipid self-diffusion is an activated process and depends strongly on temperature.

B. Local diffusivity in equilibrium is T -dependent

In ref. [18], T -independent transport arose only when the spot area of the FCS measurement was small (confocal spot area $\omega^2 = 3 \times 10^4 nm^2$). Our model membrane is smaller than this threshold, so if temperature independence were only a matter of length scale, our simulations would have captured it. However, because MSD is averaged over many ensembles and is a bulk measure, it may hide local T -independent transport processes. Hence, we investigated the transport of lipids at various length scales, ranging from individual lipids to regions containing 10-15 lipids.

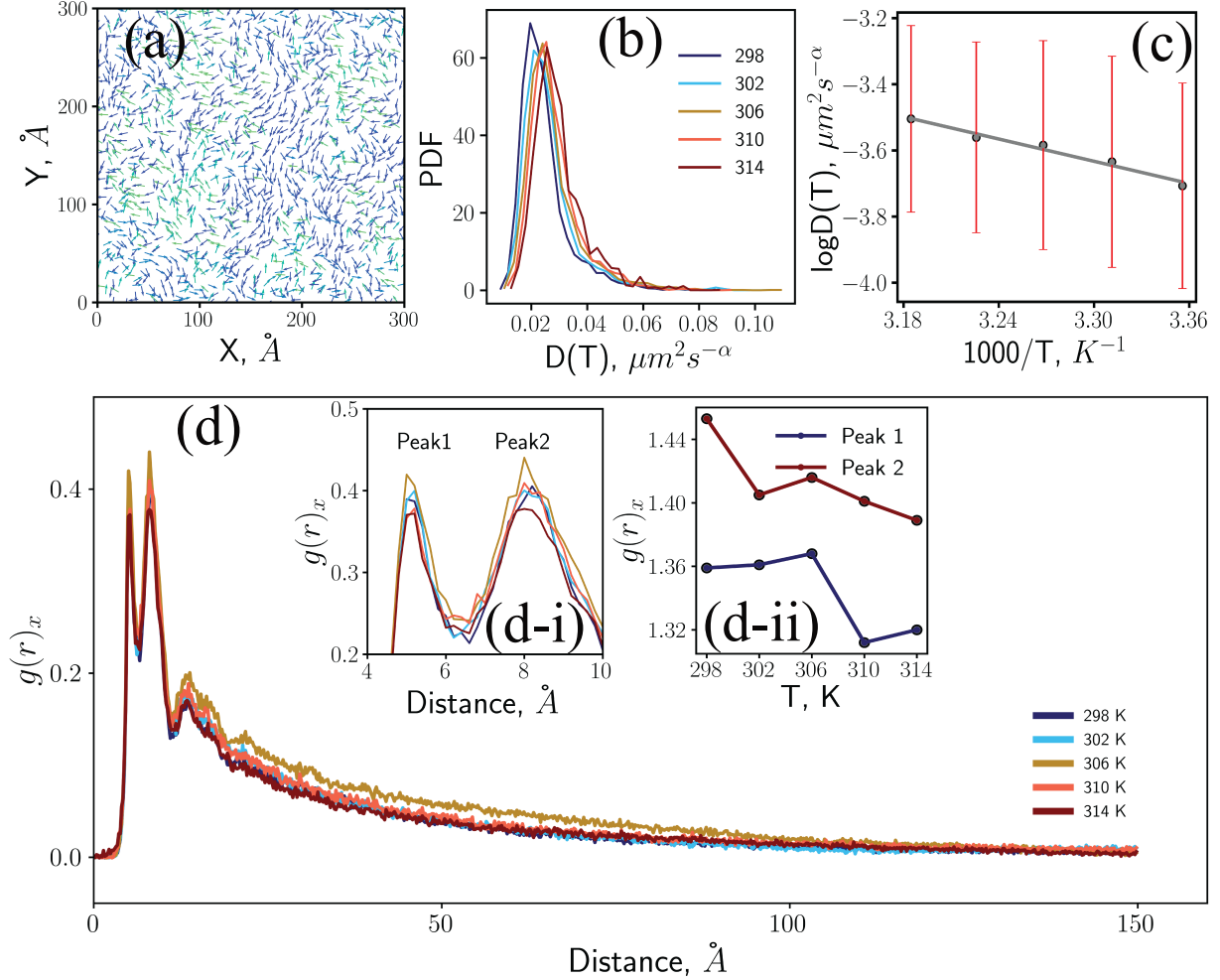


FIG. 2. Nanoscale transport of lipids is T -dependent. (a) Snapshot of lateral displacement of DPPC lipids at 314 K with $\tau = 20$ ps. (b) Probability distribution of diffusivity in the grid-box ($3 \text{ nm} \times 3 \text{ nm}$) at different T , ($\alpha = 0.55$). (c) Transport coefficient, $D(T)$ at different T in semilog scale, ($\alpha = 0.55$). (d) Displacement-displacement correlation (DDC) quantification for DPPC to its respective T . (d-i) Zoomed view of Peak 1 and Peak 2 from DDC. (d-ii) Peak height at Peak 1 and 2 with its corresponding T . All the results are from short-time scale simulations. Error bars are standard deviation of 20 replicates.

We found that individual lipids showed correlated motion with their neighbors and next-nearest neighbors when the lag time was short (ps-ns) (Fig 2a), which has also been shown before [28]. In contrast, in the long time scales where we examined ensemble-averaged MSD curves (Fig. 1a), we noticed diffusive behavior implying random movement of lipids. Therefore, the bulk, long-time behavior of the lipid transport, as seen in the MSD curves,

is strikingly different than their local short-time transport. Hence, we analyzed the local nanoscale transport through means different from ensemble-averaged MSD.

First, we measured the local diffusivities of the lipids using their MSD averaged over grids of size $3 \text{ nm} \times 3 \text{ nm}$ (Fig. S3). From these distributions, we computed the distribution of the transport coefficient, $D(T)$, at different temperatures and measured their average value. Both showed weak but clear Arrhenius-like T -dependence (Fig. 2b, c). Therefore, in equilibrium, even at the nanoscale, we observed clear signatures of activated diffusion, which consolidated our hypothesis that active driving is needed to make activated diffusion T -independent.

Because MSD based measurements of transport coefficients are defined in the $t \rightarrow \infty$ limit, it is unclear whether MSD-based measurement of $D(T)$ is accurate or not. A more accurate alternative is to measure the T -dependence through the correlation functions (see A 3) of the lipid transport. For this purpose, we measured the displacement-displacement correlation function [29–36], which showed two prominent peaks at around 0.51 and 0.83 nm distance (Fig. 2d). The peaks showed weak but systematic variation with temperature: both decreased in height with increasing temperature (Fig. 2d-i, d-ii). However, the variation is so small that it will be impossible to detect it in present experiments.

Our observations suggest that equilibrium correlated flows cannot render the transport T -independent. Hence, we conjectured that nonequilibrium flows of lipids must be the origin of T -independence in the FCS experiment. At the smallest lengthscales probed by the FCS experiments [5, 37], this nonequilibrium flow must affect tens of thousands of lipids simultaneously, indicating that the cortical ACS is a possible driver of such flows [13, 38, 39]. Unfortunately, it is tough to investigate the coupled dynamics of the ACS with the membrane using CG-MD because of the prohibitive computational cost. To the best of our knowledge, even with the best supercomputers, the interaction between membrane and only a single actin filament has been studied [40]. Hence, we resort to a mesoscopic lattice model [41] of the membrane to investigate the effect of the ACS on the membrane-lipid transport (See A 4).

C. Kawasaki algorithm gives incorrect equilibrium kinetics

Traditionally, the local Kawasaki algorithm is used to model the self-diffusion of lipids on lattice models [41–44]. However, the Kawasaki algorithm is not appropriate for modeling self-diffusion because it cares only about the energy difference between the state before and after the swap and does not care about the energies of the transition states that facilitate the move (Fig. 3a). Hence, it correctly captures thermodynamics but fails to capture the kinetics of any processes. Here, we show this discrepancy for the self-diffusion of lipids in a membrane.

In the membrane, a lipid interacts with its neighboring lipids. When two adjacent lipids swap places, there are significant rearrangements of the local lipid configurations. Such *transition states* usually have higher free energy than the configurations before and after the swap. From a modeling perspective, it implies that every lipid swap requires overcoming a kinetic barrier with activation energies correlated with the diffusing lipid’s total interaction energy with its neighbors. In Kawasaki algorithm, we ignore this activation energy. The resultant transport process is unphysical: the coefficient of self-diffusion shows nonmonotonic variations with T (Fig. 3b). For temperatures higher than 312 K, diffusivity decreases with $1/T$, and below 312 K, diffusivity increases with $1/T$, violating experimental and computational observations [17, 45, 46], where diffusivity decreases monotonously with $1/T$.

Kawasaki dynamics gives such inaccurate results because it incorrectly increases the swap rate of like lipids in lipid domains, where swapping does not cost any energy. However, because like lipids attract each other, the energetic cost of kinetic rearrangements is high, resulting in a high activation barrier. Therefore, kinetically, we expect like lipids to slow down in a lipid domain, as seen in experiments [5]. However, Kawasaki algorithm is agnostic of this cost and leads to inaccurate T -dependence at low temperatures (high $1/T$), where lipid domains form easily. At higher temperatures (low $1/T$), lipids of various species are well-mixed, and the kinetic barriers are close to zero. Hence, there, the Kawasaki algorithm predicts the right temperature dependence.

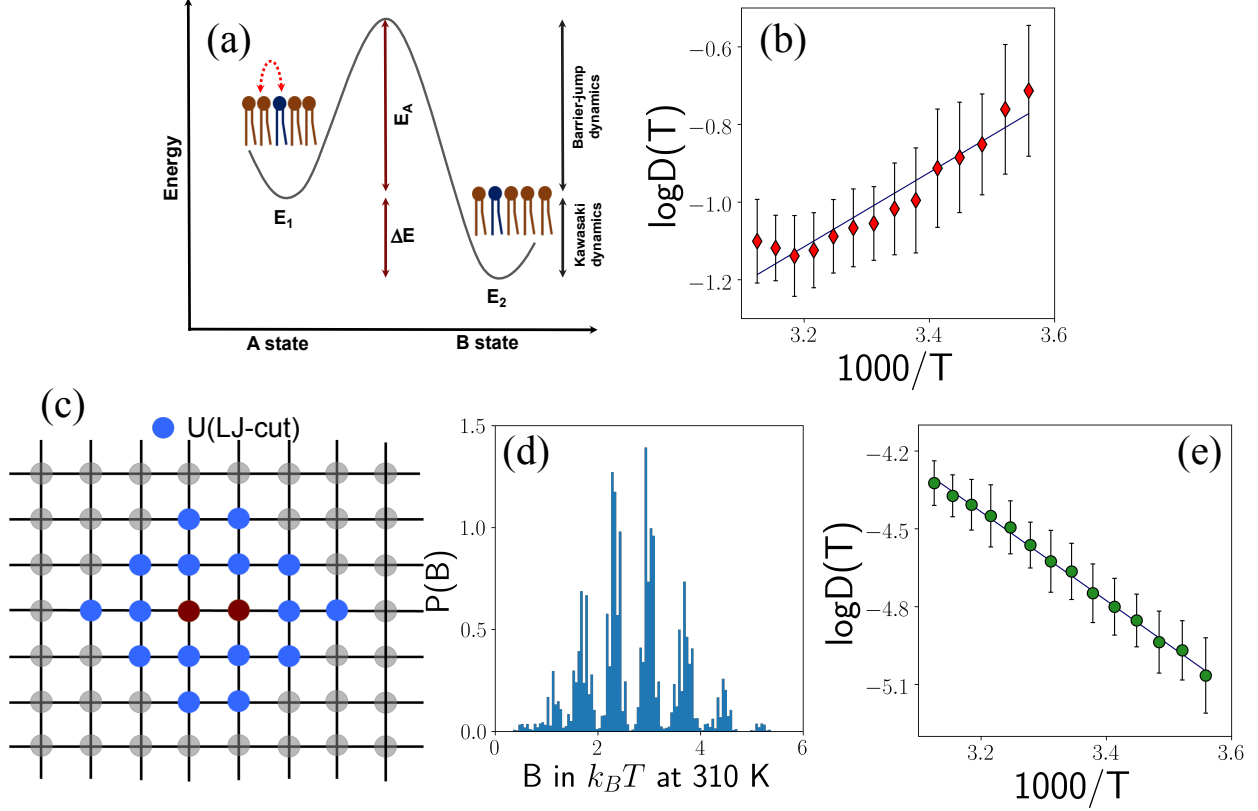


FIG. 3. (a) The energy profile diagram for the exchange process of the lipids from, let's say, A state to B state, where ΔE and E_A are the energies used in the Boltzmann factor for the Kawasaki (KD) and Barrier Hop Dynamics (BHD), respectively. (b) Kawasaki dynamics predicts unphysical variation of $D(T)$ with T . (c) Illustration of the lattice model, where maroon colored lipids at the center are undergoing exchange move and interacting with lipids in blue through truncated LJ potential. (d) The probability distribution of barrier heights ($B = -U$) in $k_B T$ at 310 K resulting from various configurations uniformly sampled (e) BHD gives us the desired activated diffusion given by Arrhenius kinetics [17] $E_A = 5.81 k_B T$ at 310K.

D. Barrier Hop Dynamics (BHD) gives correct equilibrium kinetics

To incorporate the kinetic effects into our model, we use a simplified model of activation barrier, where the barrier height is equal to the negative of the total interaction energy of the diffusing lipid as shown in Fig. 3a.

$$B = -U \quad (3)$$

We call this algorithm Barrier Hopping Dynamics (BHD). Similar algorithms have been used before to model activated processes [47]; they provide excellent qualitative insights. Incorporating more details about the transition state and the associated free energies in the model may improve the accuracy of the model, but it does not guarantee better quantitative accuracy of the results. Because the lattice model is itself an ultra-coarse-grained description of the membrane lipids, it is unclear whether it is even possible to identify correct transition states or, if possible, whether they provide an accurate description of the microscopic activation processes.

Using the BHD algorithm (see A 4 c), we model the equilibrium self-diffusion of lipids on the lattice. The lipids interact with each other through Lennard-Jones potential, from which we calculate the total interaction energy, U , of a pair of lipids (Fig. 3c). U depends on the local lipid configurations and there are $2^{18} \approx 2.6 \times 10^5$ of them. From a random sampling of these configurations, we obtain the distribution of barrier heights, which vary between 0 and $6 k_B T$ at 310 K (Fig. 3d). The self-diffusion coefficient obtained from this model follows Arrhenius kinetics with an activation barrier of $E_A = 5.81 k_B T$ at 310K (Fig. 3e), which is within a factor of three of the mixed-membrane E_A and comparable to single component membrane E_A obtained from CG-MD simulations (Fig. 1c). Therefore, in the lattice model, we have used the BHD algorithm to model all equilibrium diffusive moves.

E. Active transport of lipids is T -independent

Through its interaction with motor proteins, ACS forms dynamic spatiotemporal patterns called asters, which are roughly circular in shape [38, 41, 48]. Because of the exchange of filamentous actin between the ACS and the cytosol, called actin turnover, the asters spontaneously form and decay with a characteristic lifetime, τ_a [49, 50]. Here, we use a simplified model of aster dynamics, described in [41], to model its effect on the membrane. We assume that all asters are circular and of the same size R_a . The lifetime of an individual aster is an exponential random variable with mean τ_a . We conserve the number of asters and assume that aster creation and annihilation are uncorrelated events. Hence, as soon as an aster disappears, another aster forms at a random location [41]. To ensure the uncorrelated formation of asters, we use a sufficiently small density of asters, which does not affect our main conclusion. The effect of the asters on the membrane is captured by introducing

patches where active moves are allowed. These patches have the same size and lifetime as the aster that adjoins it. Passive lipids bind reversibly to the ACS when they are within this patch. When bound, they move persistently toward the aster core via active MC moves. When not bound, passive lipids move diffusively through BHD. Inert lipids never bind to the ACS and always move diffusively through BHD. Outside this patch, all lipids move diffusively through BHD (see A5)

The appearance and disappearance of the asters introduce active fluctuations in the lipid movement, which changes their transport properties. To illustrate this change, we studied an extreme system where the passive lipids, once inside an aster patch, remained always bound to the aster and moved only through active moves. We found that the MSD of the passive lipids showed negligible T -dependence (Fig. 4a), implying the T -independence of $D(T)$ (Fig. 4a-inset). Therefore, our hypothesis that active fluctuations lead to T -independent diffusivity seems correct.

To check whether such weak variation can be captured in experiments, we computed the Q_{10} metric [18, 51]. To have significant T -dependence Q_{10} must be greater than 1.2 [18]. However, we found that Q_{10} for the passive lipids was lower than this threshold. Hence, its T -dependence will not be detected in experiments.

The inert lipids, which never couple to the ACS, also show altered transport properties, with weak superdiffusive behavior at small τ and weak subdiffusive behavior at large τ as shown in Fig. 4b. Therefore, to investigate the T -dependence of the transport, we cannot use diffusivity and must use a general transport coefficient. In general, we can write:

$$\langle X^2 \rangle = 4D(T)\tau^\alpha, \tag{4}$$

where $\langle X^2 \rangle$ is the MSD, α is the anomalous diffusion exponent, and $D(T)$ is a transport coefficient equal to the diffusivity when $\alpha = 1$. We use this general definition of the transport coefficient, $D(T)$, to quantify the T -dependence of the lipids. As shown in Fig. 4b-inset, $D(T)$ for inert lipids shows a much stronger dependence on temperature than the passive lipids. This observation consolidates our hypothesis that ACS activity is the driver of T -independent transport, and it also shows that the transport of a lipid can be affected even when it does not interact with the ACS directly.

To test our hypothesis further, we systematically reduced the binding probability, p_b of the passive lipids with the ACS. We found that for low p_b , the equilibrium T -dependence was

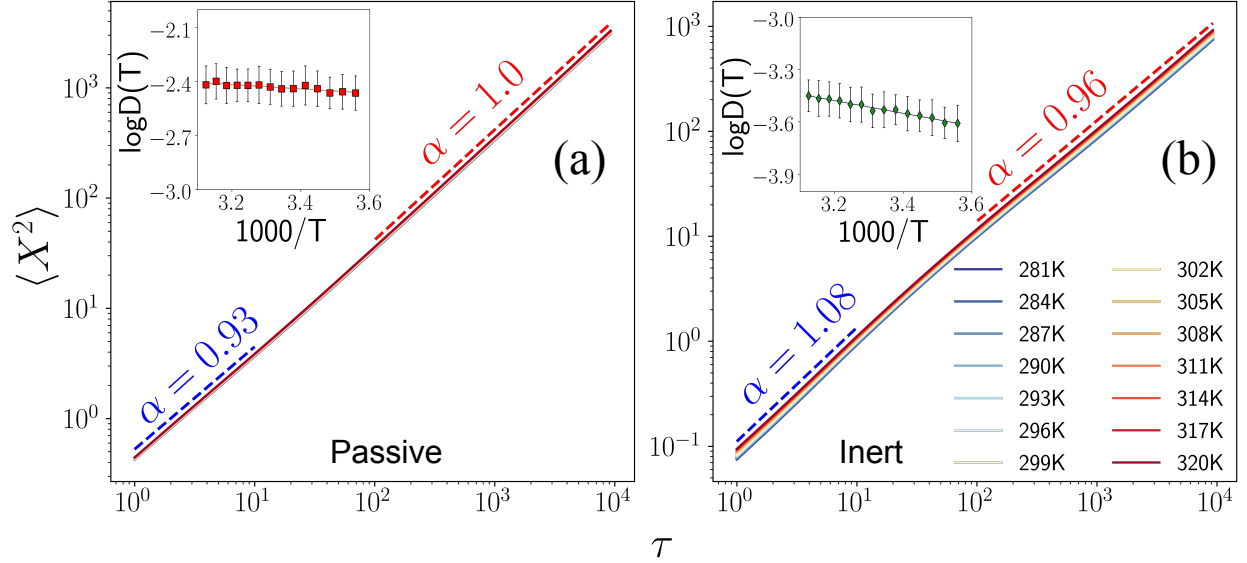


FIG. 4. MSD, $\langle X^2 \rangle$, vs lagtime τ for passive and inert lipids for $p_b = 1$. (a) Passive lipids are subdiffusive at timescales comparable to average aster remodeling time and become diffusive at timescales longer than that. Inset: $\log D(T)$ vs $1000/T$ shows that the transport coefficient is nearly T -independent for passive lipids. (b) Inert lipids, in contrast, show a transition from weakly superdiffusive to weakly subdiffusive transport at the same timescale. Inset: For inert lipids, $D(T)$ increases exponentially with T . The T -(in)dependence is also evident from the spread of the MSD curves with T .

recovered, with the exponential variation of $D(T)$ with temperature for both passive and inert lipids (Fig. 5). At high p_b , $D(T)$ became T -independent for passive lipids and weakly T -dependent for inert lipids. These observations provided the final confirmation that active, nonequilibrium, fluctuations are responsible for T -independent transport in our system.

F. Transport of inert lipids

As shown in Fig. 4, the transport of inert lipids is superdiffusive at short τ , even though there is no direct coupling to the active movements. We hypothesized that superdiffusion arises indirectly due to the excluded volume interaction between inert and passive lipids and the directed movement of the passive lipids in an aster. Before an aster forms, both types of lipids are equally likely to be present in a given region. However, when an aster forms, the passive lipids are more likely to cluster around the aster cores because of their

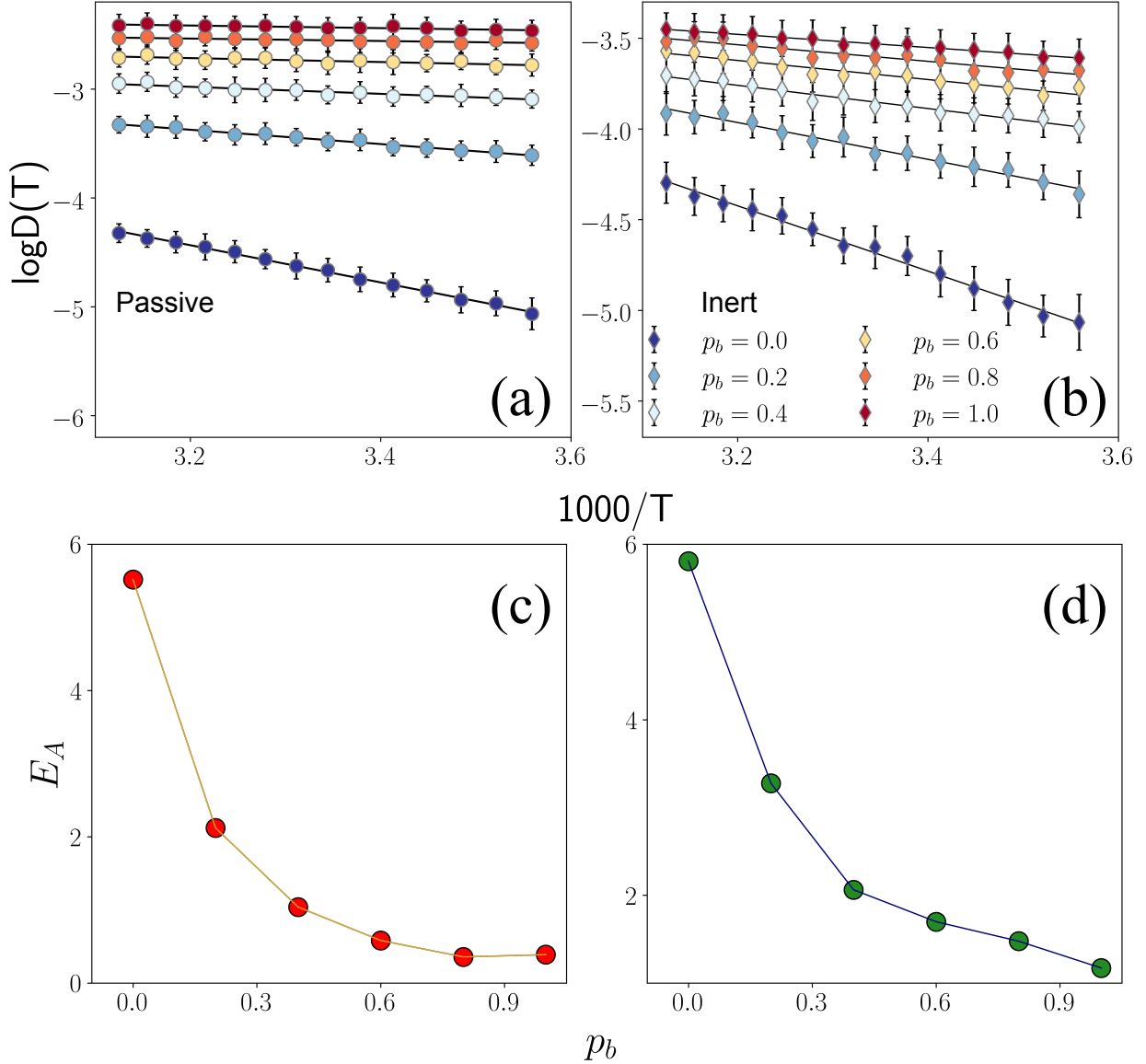


FIG. 5. Effect of finite binding affinity between the passive lipids and the ACS. (a) $D(T)$ for passive lipids for different p_b . T -dependence is recovered at lower p_b . (b) $D(T)$ for inert lipids shows stronger variation with T . (c) E_A for passive lipids, and (d) E_A for inert lipids. E_A decreases with increasing p_b , that is transport becomes more T -independent with increasing p_b .

directed movement towards the core and the expulsion of the inert lipids from the core due to excluded volume interaction. To test this idea, we created a system where asters form only in a small region at the center of the lattice (R_1). Both passive and inert lipids populate R_1 , whereas only inert lipids populate the area outside this subsystem (R_2) as shown in Fig. 6a. After a sufficiently long time, we observed distinct transport behavior

of inert lipids in regions R_1 and R_2 . Because R_1 resembles the lattice model we have used so far, we expect the MSD of the inert lipids in R_1 to be similar to Fig. 4b. Whereas in R_2 , they only diffuse with the BHD moves, which should make the transport the same as in an equilibrium system, with strong T -dependent activated diffusion. We indeed observe the same dependence for MSD (Fig. 6b). Moreover, the $D(T)$ looks strikingly different in the two regions: it is almost T -independent in R_1 but shows strong T -dependence in R_2 (Fig. 6c). Therefore, the indirect coupling between inert lipids and ACS via passive lipids leads to the altered transport of the inert lipids, leading to its weak T -dependence.

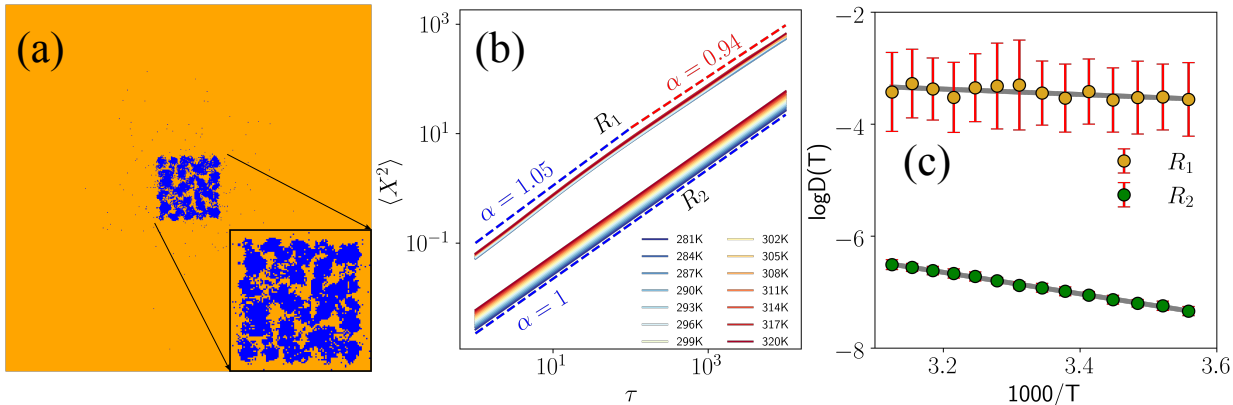


FIG. 6. Transport of inert lipids in a composite region. (a) The snapshot shows the entire simulation box 500×500 grids, and the region in the middle (and the zoomed-in inset) is R_1 (100×100 grids). Regions outside R_1 is R_2 . Inert lipids are shown in orange, and passive lipids are shown in blue. R_1 contains both passive and inert lipids and R_2 contains only inert lipids. (b) MSD, $\langle X^2 \rangle$, vs τ (lag time) and (c) $\log D(T)$ vs $1000/T$ for $T \in [281K, 321K]$ for inert lipids in the two regions.

It is worthwhile to make some comments about membrane transport of lipids in light of these observations. First, lipids may move superdiffusively at short times even when they are directly not coupled to active driving forces. Hence, when developing reaction-diffusion-type models for membrane transport, we need to be aware of this fact. Second, as noted earlier [41], lipid segregation is enhanced in the presence of ACS-driven active fluctuations, which may help cells maintain membrane homeostasis in the presence of thermal shock or when thermal fluctuations are not sufficient to create segregated membrane structures, such as lipid rafts.

III. DISCUSSION

Cells have evolved to deal with their noisy environment. How a cell maintains the robustness of its machinery from the continuous assault of thermal noise has been a matter of extensive investigation [52–56]. These studies have repeatedly shown that nonequilibrium driving forces can significantly improve a cell’s ability to function. In this paper, we investigate how the transport of molecules, which control and coordinate all cellular processes, are protected against thermal fluctuations.

We have made two striking observations. First, at the nanometer scale, the flow of the lipids is strongly correlated yet shows clear signs of activated diffusion. On the other hand, the macroscopic activated diffusion of lipids shows no such correlated movements. Where the microscopic correlation is lost is unclear. It is puzzling that even though the lipid movements are strongly correlated at the nanoscale, the standard metric of transport, such as the MSD or the diffusion coefficient, does not show it. A theoretical study would require understanding the many-body transport of lipid clusters that move together at the nanometer scale. The collective motion of the lipid clusters may be random, which is why, perhaps, the MSD or the diffusion coefficient does not capture it. However, we do not have any proof for this hypothesis. We are also unsure about the origin of the weak T -dependence in lipid self-diffusion at nanosecond timescales, where such correlated motion is observed. At that scale, it is difficult to calculate the transport coefficients unambiguously, as they are defined in the $\tau \rightarrow \infty$ limit.

The second striking observation is that nonequilibrium flow from the ACS makes the transport coefficient, $D(T)$ weakly T -dependent. Even though we have demonstrated this T -independence for a particular nonequilibrium driving, namely the presence of the ACS, it is easy to see that our model is not fine-tuned to any specific biological system. Instead, the key ingredient is the stochastic switching between active and passive moves. As shown in Fig. 5, reducing the propensity of the active moves to the passive moves increases T -dependence. Therefore, the T -independence of $D(T)$ originates from the breaking of detailed balance and is a general observation that is not surprising by itself. Indeed, it is well-known that the fluctuation-dissipation theorem, which relates a transport coefficient to the ambient temperature, is generally violated far from thermal equilibrium [8, 57, 58]. What is remarkable is that the T -independence of $D(T)$ provides a novel mechanism to ensure the

robustness of cell signaling.

Specifically, let's consider the precision of molecular sensing on the cell membrane in the slow diffusion (fast reaction) limit, where the precision of sensing concentration, c , of a ligand [59] varies as

$$\epsilon(T) = \frac{\delta c}{c} \propto \sqrt{\frac{1}{D(T)}} \quad (5)$$

Therefore, the precision will decrease exponentially with decreasing temperature in passive membranes, where $D(T) = D_0 e^{-E_A/k_B T}$. For example, consider the precision of ligand detection in a mixed membrane, for which $E_A = 14k_B \times 310K$ (Fig. 1c). We have assumed that the ligand has transport properties similar to those of DPPCs. The precision of detection at 300K will be:

$$\epsilon(300)/\epsilon(310) = \sqrt{D(310)/D(300)} \quad (6)$$

$$= \sqrt{\exp(-14 + 14 * 310/300)} \quad (7)$$

$$\approx 1.26 \quad (8)$$

That is, there will be a 26% increase in the sensing error. While this is not a dramatic increase in sensing error for an individual receptor, the collective errors are additive and can dramatically alter the precision of signaling. In contrast, $D(T)$ does not change for the active membrane, and the precision remains unchanged over a broader range of temperatures. Hence, we believe T -independent transport can provide a potential safeguard against temperature fluctuations.

T -independence in our model arises generically when lipids are transported through correlated flows. Hence, we have reasons to believe that this observation is general. However, it is important to note that our model does not explore all possible variations that can be imagined. For example, we have made the simplifying assumption that all asters are of the same size. In contrast, existing data suggest that asters have a nontrivial size distribution [60]. Our data shows that changing the size of the asters, without changing the area fraction, does not change the results qualitatively because it does not change the ratio of the active to passive moves (Fig. S4). In contrast, it is unclear whether the correlated spatial creation and annihilation of the asters can change the results qualitatively. Because it does not change the ratio of the active to passive moves, we have reasons to believe that it should not change the results qualitatively.

Finally, we have used a new algorithm called barrier hopping dynamics (BHD) to simulate diffusion. We have shown that Kawasaki dynamics, the default choice to model lattice diffusion, does not reproduce the qualitative features of equilibrium diffusion, but BHD does. We have demonstrated that Kawasaki dynamics gives unphysical transport properties. Although BHD reproduces the general features of the equilibrium $D(T)$, the choice of the barriers in this paper is unphysical. That being said, the purpose of introducing BHD was to reproduce the general features of lipid diffusion in thermal equilibrium, which we succeeded in. However, an appropriate choice of diffusion barriers would have allowed us to make quantitative comparisons with the CG-MD model calculations.

Irrespective of these drawbacks, our calculations provide valuable insights about the transport of lipids on the plasma membrane. It is surprising that even lipids not coupled to the ACS can have $D(T)$ that is almost T -independent. As we have shown, a consequence of such temperature-independent transport processes is the robustness of cell sensing. Because of their ubiquity, transport affects not just sensing but all cellular processes. Therefore, it is not hard to imagine that their temperature independence will impact the stability of all cellular processes.

IV. CODE AVAILABILITY

The in-house scripts for the calculation of MARTINI lipid simulation and lattice simulations are available open-source at [github-transport-on-active-membrane](#)

V. ACKNOWLEDGEMENTS

The Supercomputer Education and Research Center, Indian Institute of Science, Bangalore, India, provided the supercomputer facilities (Param Pravega) to carry out our CG Martini simulations. SGV thanks for the support received through the institute fellowship (010302101122122049) and PMRF fellowship (0202994). AM thanks IISc-IoE fellowship (IE/REAC-22-0112) for funding. SS thanks IISc, Axis Bank Center for Maths and Computing, and SERB-DST (SRG/2022/000163) for funding. The authors would also like to thank Somaditya Santra and Soumyadeep Mondal for their insightful discussions.

Appendix A: Methods

1. CG Molecular Dynamics

a. System

For the equilibrium simulation of PM models using CG-MD, we have used three symmetric model membranes with box size $30\text{ nm} \times 30\text{ nm}$. The models were built using the INSANE martini tool [61] and simulated in GROMACS using MARTINI 3.0 force-field to achieve faster dynamics [62, 63]. Two membranes were built using pure lipids: (1) the saturated DPPC (di-palmitoyl phosphatidylcholine, $C_{16:0}$) and (2) the polyunsaturated DAPC (di-arachidonoyl phosphatidylcholine, $C_{20:4}$). A third mixed composition membrane (DPPC: DAPC: CHOL, 5:4:3) was also simulated to understand lipid transport in more realistic membranes [64]. All systems were solvated with water, and 0.15 M NaCl was added to attain the physiological ionic condition [61]. The system topologies were created in the GROMACS format. Five different temperatures (298, 302, 306, 310, and 314 K) were used to check T dependency of the PM models. All the production simulation (Table. I) was conducted for $5\ \mu\text{s}$, except two pure DPPC systems that were run for $30\ \mu\text{s}$ using GROMACS-2022.2 [65–67] with 20 fs timestep where each 100 ps snapshots were stored for analysis. The detailed simulation protocol is given in the SI.

PM	Replicas	Time ($\mu\text{s}/\text{run}$)	Time ($\mu\text{s}/\text{temp}$)	Total Time (μs)
Pure DPPC	2	30	60	300
	6	5	30	150
Pure DAPC	10	5	50	250
Mixed	12	5	60	300
Total				1000

TABLE I. Simulation Details

b. Lipid flow simulation

Another set of simulations was conducted to study the nanometer scale correlated flows of lipids. The T range was kept the same (298-314 K), and only the pure DPPC model was simulated. The starting structures were taken from the long simulations (after 3 μ s) to their respective temperatures. All the parameters were kept the same, but the run time was reduced to 1 ns with 20 fs timesteps. These short-time simulations were run for 20 replicas at each temperature, and each 20 fs coordinates were stored.

c. Analysis

The analysis was conducted with in-house developed Python 3.11 programs using the MDAnalysis package [68] and GROMACS-2022.2 tools [67] and visualization was performed with the molecular graphics viewer VMD [69].

2. MSD calculation

To understand the T -dependence of the lipid transport, we have employed various analysis protocols to measure the diffusivities of lipids.

a. Bulk diffusivity measurement

The MSD for lipids at different temperatures was calculated over the last 2 μ s of each 5 μ s runs, whereas the last 5 μ s were used for the 30 μ s trajectories. The analyzed part of the trajectories was further divided into 1 μ s blocks [70, 71] to calculate MSD. The MSD is defined as:

$$\langle X^2 \rangle = \langle |\mathbf{r}_i^\tau - \mathbf{r}_i^0|^2 \rangle = \frac{1}{N} \sum_{i=1}^N [(x_i^\tau - x_i^0)^2 + (y_i^\tau - y_i^0)^2], \quad (\text{A1})$$

where $\langle X^2 \rangle$ is the MSD, N is the number of particles in the system, x_i^τ , y_i^τ and x_i^0 , y_i^0 is the position of the i^{th} particle on XY plane at times τ and 0, respectively.

The `gmx msd` tool was used to calculate the MSD of the PO_4 (PC lipids) and ROH (for CHOL) beads of the lipids (only the headgroup of lipids were considered for the MSD calculation). The results were plotted on a log-log scale to determine the power-law dependence of

diffusion. The diffusion or transport coefficient was calculated by multiplying the slope with the coarse-grained (CG) conversion factor of 4, as suggested in [72, 73]. Subsequently, the transport coefficients at different temperatures were plotted to derive the activation energy of specific lipid molecules using the Arrhenius equation:

$$D(T) = D_0 e^{-\frac{E_A}{k_B T}}, \quad (\text{A2})$$

$$\ln D(T) = -\frac{1}{T} \frac{E_A}{k_B} + \ln D_0, \quad (\text{A3})$$

where D_0 is a T -independent constant that depends on the lipid properties, k_B is the Boltzmann constant, and E_A is the activation energy. E_A was determined by calculating the slope of $\ln D(T)$ vs $1/T$ curve for different PM models. Per experimental convention, $1000/T$ was used instead of $1/T$ for the plots [17]. The errors were estimated from the standard deviation among the replicas.

b. Local diffusivity measurement

To understand the short-time spatial behavior of lipids, we analyzed one ns simulation trajectories. The system was divided into grid boxes measuring $3 \text{ nm} \times 3 \text{ nm}$, each containing approximately 10-15 PO_4 beads of DPPC lipids, which were tracked to measure the local MSD (Fig. S3). The lag time τ was varied between 0 and 1 ns with a resolution of 20 fs. The time-averaged MSD for the PO_4 groups within each grid box was computed, which showed subdiffusive transport with the anomalous exponent of 0.6. Therefore, the transport coefficient was not the diffusion constant. However, we could still determine the transport coefficient, $D(T)$, from the slope of the MSD curve (check the results section for details). Following the $D(T)$ calculation, we analyzed its distribution across the grids for the abovementioned temperatures. This method was repeated for the remaining replicas, and we compared the spatial average of $D(T)$ at different T .

3. Correlation analysis

To accurately quantify the correlation in the lipid displacements (see results), we measured the displacement-displacement correlation (DDC) function for DPPC [31, 35, 36]. DDC generally reveals the degree of dynamical heterogeneity in the system, indicating the

spatial distribution of its mobile elements [32, 33]. DDC is used extensively to quantify dynamical heterogeneity in the glass transition [29, 30, 34].

On a fixed time interval τ , the displacement vectors for the i^{th} and the j^{th} lipids, $\hat{x}_i(r_i, \tau)$ and $\hat{x}_j(r_j, \tau)$ were calculated. The correlation function is then given by:

$$g(r, \tau)_x = \frac{1}{N} \sum_{i=1}^N \sum_{j=1}^N \langle \hat{x}_i(r_i, \tau) \cdot \hat{x}_j(r_j, \tau) \delta(r - |r_{ij}(t_0)|) \rangle, \quad (\text{A4})$$

where N is the number of particles in the system, $r_{ij}(t_0)$ is the initial separation distance between i^{th} and the j^{th} lipids.

4. Lattice model simulation

In the lattice model [41, 43, 44], every grid is occupied by a lipid species that either couple to the underlying ACS or does not couple. We assume that the lipid that couples to the ACS does not influence its behavior, and it gets *passively* transported by the ACS. Following the terminology of ref. [38], we call them *passive* lipids. The lipids that do not interact with the ACS are called *inert* lipids. The lattice model is a coarse-grained model, and each grid is averaged over many molecular lipids. Therefore, the passive-inert classification has to be judged based on the net interaction of the lipids in a grid. Our lattice model can, in principle [74, 75], be derived from a systematic coarse-graining of a detailed molecular model, which is beyond the scope of the current paper. Here, we assume that such a coarse-graining is possible, and the effective interaction between the lattice-lipids is of similar strength as that between two molecular lipids, which are of the order of $0.5 k_B T$. In doing so, we lose all the chemical details of the CG model, which constrains us from providing any legitimate macroscopic thermodynamic information about the ACS-lipid interaction. However, the lattice model can provide a qualitative understanding of the transport process in the presence of ACS, even when detailed molecular information is missing. Unless otherwise stated, from now on, we use the term lipids to imply the lattice lipids when talking about the lattice model.

a. Interaction between lipids

Lipids of the same type (passive-passive or inert-inert) interact with each other through attractive Lennard-Jones (LJ) potential $U(r) = -J(\frac{\sigma}{r})^6$ with a cutoff radius of 2.5σ , where we took one lattice unit as $2^{1/6}\sigma$ for excluded volume interaction between unlike lipids. Hence, we have at most two lattice units ($= 2 \times 2^{1/6}\sigma < 2.5\sigma$) attractive interaction between like lipids as shown in Fig. 3c. The interaction strength J is chosen so that $J/k_B T = 1/1.43$ at $T = 293 \text{ K}$. Lipids of different species interact with excluded volume interaction only, such that $J = 0$ for unlike lipids. Hence, the total interaction energy, U , of a given pair of lipids varies between -6 to $0 \text{ k}_B T$, which is in the same ballpark as the activation energies calculated from the molecular simulation. The neighbor configurations and the interaction energy distribution ($-U$) for different possible neighbor configurations are shown in Fig. 3d.

b. Equilibration

To equilibrate the lipids on the lattice, we used Kawasaki exchange moves [47], which exchange two neighboring lipids with a probability p determined by the following formula:

$$p = \begin{cases} 1 & \text{if } \Delta E \leq 0 \\ e^{-\Delta E/k_B T} & \text{if } \Delta E > 0, \end{cases} \quad (\text{A5})$$

where ΔE is the difference in the interaction energy before and after the swap. Kawasaki moves guarantee the system reaches the correct equilibrium state if runs sufficiently long. However, due to kinetic effects, *local* Kawasaki moves often lead to an arrested state. Hence, we used *global* Kawasaki moves for equilibrating a random initial lipid configuration. In the global algorithm, two lipids were chosen randomly from the entire system and swapped using the same criteria, which avoided the kinetic traps and rapidly converged to the global equilibrium state at a given temperature.

c. Diffusive (passive) moves

The equilibrated state served as the initial condition for the simulations to study the transport of the lipids.

The algorithm, which we call *barrier hopping dynamics* or BHD, is as follows:

1. Pick a random lipid and a neighboring lipid
2. Calculate the total interaction energy of the lipid and the neighboring lipid, U .
3. Measure the barrier height $B = -U$.
4. Swap the lipids with probability $p = e^{-B/k_B T}$.

Barrier heights chosen this way are unrealistic as they do not capture the various entropic effects that determine the free energy of the transition state. Obtaining the “correct” barrier heights would require detailed molecular simulation followed by systematic coarse-graining of the barrier heights, which is beyond the scope of this manuscript [74, 75]. Instead, our model provides a simple alternative that can be used to understand the effect of active fluctuations on lipid transport, which is the main focus of this paper. Indeed, similar models have been used previously with similar intentions [47, 76, 77]. Another concern is that if U is positive, such as in the presence of long-range repulsive forces, B will become negative. There, we need to identify a better definition for B . Here, we do not consider long-range repulsive forces, and B is always non-negative.

5. Detailed-balance breaking active moves

Because of the interaction of the motor proteins with the ACS, various out-of-equilibrium structures form spontaneously. One of the most prominent structures is the asters, radially symmetric concentrations of actin filaments, typically ~ 100 nm in size. It has been shown that the asters are central hubs of PM-ACS interaction [38]. Therefore, in the lattice model, we consider the effect of asters on the lipid transport on the plasma membrane. Specifically, we assume the asters are disk-like dynamic regions on the membrane, where the lipids can be transported via active moves. The details of the aster dynamics are outlined later.

Once a passive lipid is inside the circular region defined by the aster, it can be advected by active moves if it also binds to the ACS. Because passive lipids stochastically bind to the ACS, we assume that the passive lipids have some binding probability, p_b , which controls how often they bind to the ACS. A passive lipid bound to the ACS is advected to its core [41]. The detailed algorithm and simulation parameters are given in the SI.

a. Aster Remodeling

Simultaneously with lipid dynamics, asters follow life-death processes with remodeling rate(τ_a) such that the area fraction of asters (A_{frac}) remains constant. The number of aster discs at any time is the same and defined by $N_{aster} = \frac{A_{frac}L^2}{\pi R_a^2}$. Once asters are initialized, a lifetime (t_{life}) sampled from an exponential distribution with mean lifetime (τ_a) [50] is designated to each aster from the time of birth (t_{birth}). No overlap between asters was ensured while carrying out the aster birth-death process. When $t - t_{birth} = t_{life}$ aster disappears and appears with some other independent location and lifetime.

6. Algorithm for active moves

The detailed balance-breaking or active moves are implemented on the lattice through Kinetic Monte Carlo exchange moves, slightly modified from [41]. The algorithm chosen to perform the exchange move is as follows:

1. A lipid is chosen randomly from $L \times L$ sites.
2. Next, a neighbor is chosen for the exchange.
 - If the chosen lipid is passive and is bound to the ACS (with binding probability p_b), then the neighbor lipid for exchange is selected to lie in the aster core direction with probability $p > 0.25$. Other neighbors are chosen with probability $(1 - p)/3$.
 - Otherwise, any of the four neighboring lipids are chosen with equal probability.
3. p_b is defined from the two-state model of the (un)bound states of passive lipid with ACS. Hence, $p_b = 1/(1 + e^{\frac{\Delta E}{k_B T}})$, where ΔE is the energy difference between the bound and the unbound state.
4. Let \vec{r}_i , \vec{r}_f and \vec{r}_a be the position vectors of the chosen passive lipid, neighbor site for exchange, and the aster core, respectively. To perform the directional move on the lattice, we have defined three cases from $\vec{r}_a - \vec{r}_i = \Delta\vec{r} = \Delta x\hat{x} + \Delta y\hat{y}$, where $\Delta\vec{r}$ is the position of aster core w.r.t the chosen passive lipid.
 - (a) $|\Delta x| > |\Delta y|$: The position of exchange site is given by, $\vec{r}_f = (x_i + \text{sign}(\Delta x), y_i)$.

- (b) $|\Delta x| < |\Delta y|$: Similarly, $r_f^{\vec{r}} = (x_i, y_i + \text{sign}(\Delta y))$.
- (c) $|\Delta x| = |\Delta y|$: The direct diagonal move is not possible. Therefore, $(x_i + \text{sign}(\Delta x), y_i)$ or $(x_i, y_i + \text{sign}(\Delta y))$ is chosen randomly.
5. Also, passive lipids near the outer aster edge feel interaction with ACS, and radial move is performed with probability $(1 - p_X)p_b$ where X is the species lying on the aster core before the swap. $p_X = 0$ if X is an inert lipid, else it is p_b .
 6. If a passive lipid is found on the aster core, it cannot move on its own, and no exchange move was performed.
 7. For passive lipids away from any aster, BHD move is performed.

Supplementary Information: Self-diffusion is temperature independent on active membranes

Saurav G. Varma, Argha Mitra, Sumantra Sarkar

Center for Condensed Matter Theory, Department of Physics, Indian Institute of Science, Bengaluru, Karnataka, 560012

I. CG-MD SIMULATION PROTOCOL

a. Energy minimization and equilibration: The system’s energy was minimized using the steepest descent and the conjugate gradients methods in the next step. We ran at least 5000 steps of energy minimization to ensure proper geometry and to minimize steric clashes. Following energy minimization, all systems were subjected to a six-step equilibration protocol (Table: SI), where the stiffness of the positional restraint on the lipid head groups (PO_4 bead of DPPC and DAPC) was gradually decreased to avoid collapse of the system. Five different temperatures (298, 302, 306, 310, and 314 K) were controlled by velocity-rescale thermostats [78] with a coupling constant of 0.1 ps, which was used. For the equilibration, we used Berendsen barostat [79] with the compressibility of $4.5 \times 10^{-5} \text{ bar}^{-1}$ semi-isotropic scaling [73, 80].

Step	Restraint ($KJmol^{-1}s^{-1}$)	Timestep (fs)	Time (ns)
1	200	2	1
2	100	5	1
3	50	10	1
4	20	15	0.75
5	10	20	1
6	2	20	50
Total			54.75

TABLE SI. Equilibration Details

b. Production runs: For these simulations velocity rescale temperature bath was applied [78]. The pressure was controlled with the Parrinello-Rahman barostat [81] with a 12 ps coupling constant, and the compressibility of $3 \times 10^{-4} \text{ bar}^{-1}$ [82]. However, due to the

longer spatial scale during production, the chance of undulation increases, which was significantly reduced by using a mild positional restraint ($2 \text{ kJmol}^{-1}\text{nm}^{-1}$) on the PO_4 beads in the Z-direction [70, 83]. All the production simulation was conducted for $5 \mu\text{s}$, except two pure DPPC systems that were run for $30 \mu\text{s}$ using GROMACS-2022.2 [65–67] with 20 fs timestep where each 100 ps snapshots were stored for analysis. The cumulative simulation time was 1 ms.

II. LATTICE MODEL SIMULATION PARAMETERS

Simulation parameters	Values
Lattice size ($L \times L$)	100×100
Radius of aster (R_a)	8
Areal density of asters (A_{frac})	0.2
Mean lifetime of aster remodeling (τ_a)	10
Equilibration steps	500 steps
Time to reach steady state	1000 steps
Production run	18500 steps
No. of replicas for each (T)	40
Probability to move towards aster core (passive lipids) (p)	0.8
Temperatures (T)	281 - 321K (spacing = 3K)
Binding probability of ACS to PM (p_b)	0.0 - 1.0 (spacing = 0.2)
Interaction strength of LJ ($J/k_B T$ at T=293 K)	1/1.43 (like lipids) & 0 (unlike lipids)
LJ interaction cutoff radius	2.5σ
1 lattice unit	$2^{1/6}\sigma$

TABLE SII. The mesoscopic lattice model simulation is performed on a 2D square lattice of size $L \times L$ with periodic boundary conditions. The lattice sites are occupied with either passive or inert lipids in equal ratios. All spatial parameters are in the units of lattice constant and time scales are in the units of MC steps. 1 lattice unit (σ_d) = $2.5/100 \mu\text{m}$ [41] and 1 MC step (τ_d) = $\frac{\sigma_d^2}{4D} = 0.446$ ms, where $D \sim 14 \mu\text{m}^2\text{s}^{-1}$ is the typical diffusivity value from our CG-MD simulations.

III. MOVIE DETAILS

Movie: "displace_with_activity.mp4" shows the active dynamics of lipids on a lattice at 311 K. The passive lipid densities are shown in red and the inert lipid densities are shown in blue. Passive tracer lipid tracks are shown in maroon and inert tracer lipid tracks are in blue. Asters are marked by black circles.

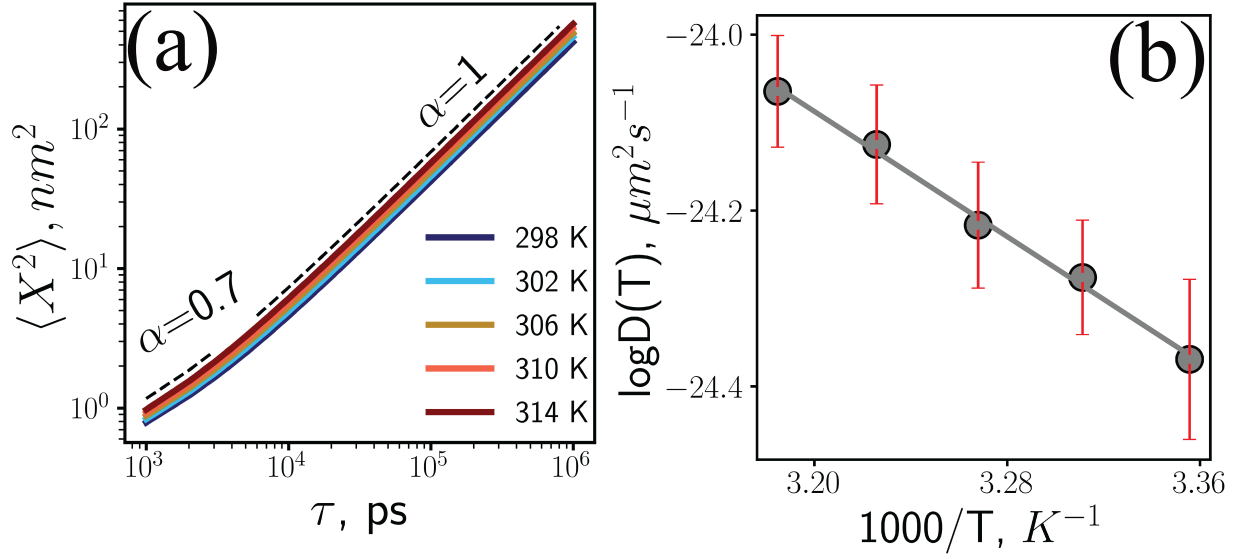


FIG. S1. In equilibrium, DAPC lipids show diffusive behavior, and the diffusion coefficient follows Arrhenius kinetics. (a-b) MSD ($\langle X^2 \rangle$) and diffusivity (semilog scale) of pure DAPC membrane at different T (298 K - 314 K). All the results from long-timescale simulations. Error bars are the standard deviation of 10 replicates.

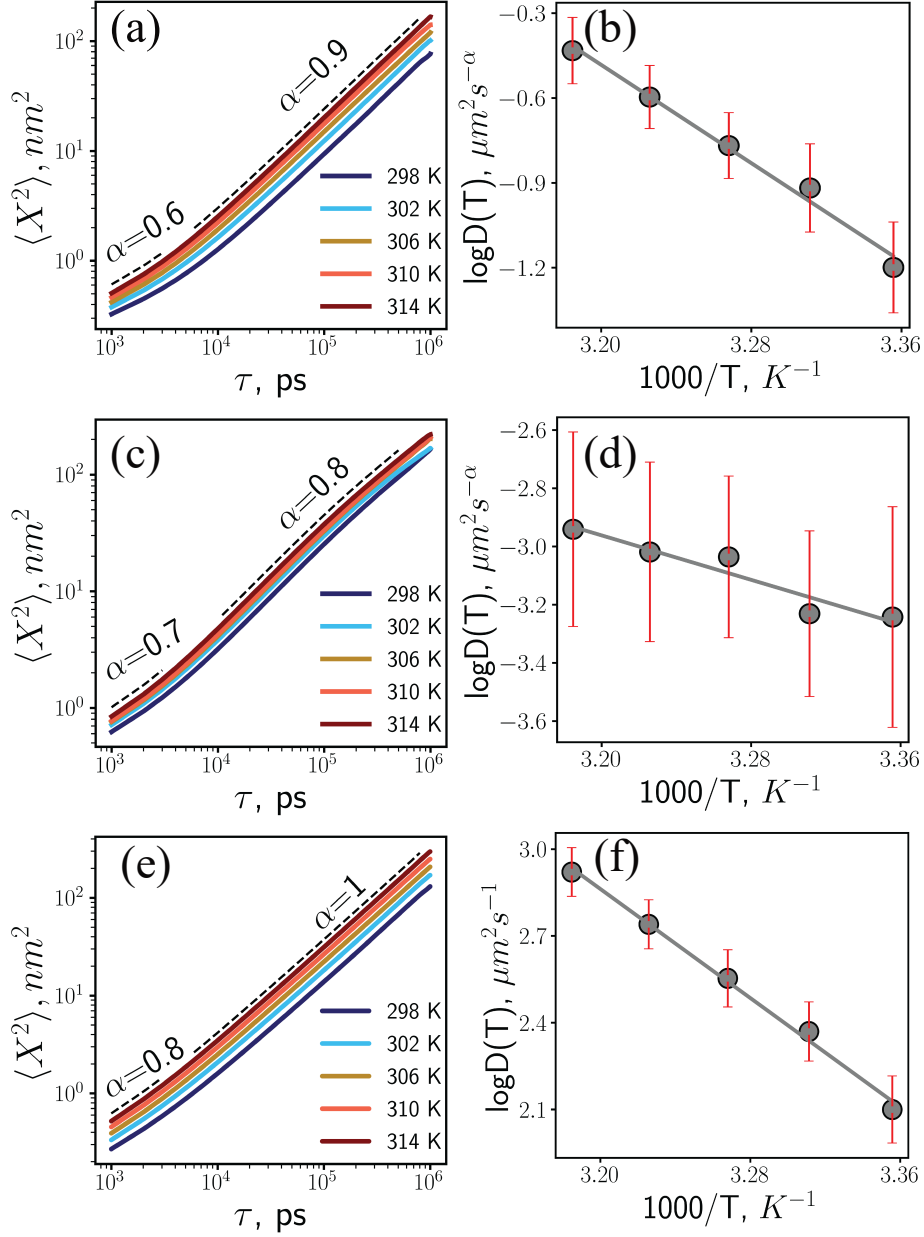


FIG. S2. In equilibrium, mixed model PC lipids show subdiffusive behavior (For DPPC, $\alpha = 0.9$ and DAPC, $\alpha = 0.8$) and CHOL shows diffusive behavior. MSD ($\langle X^2 \rangle$) and transport coefficient (semilog scale) of DPPC (a-b), DAPC (c-d), and for CHOL (e-f) in the mixed model membrane at different T (298 K - 314 K). All the results from long-timescale simulations. Error bars are the standard deviation of 12 replicates.

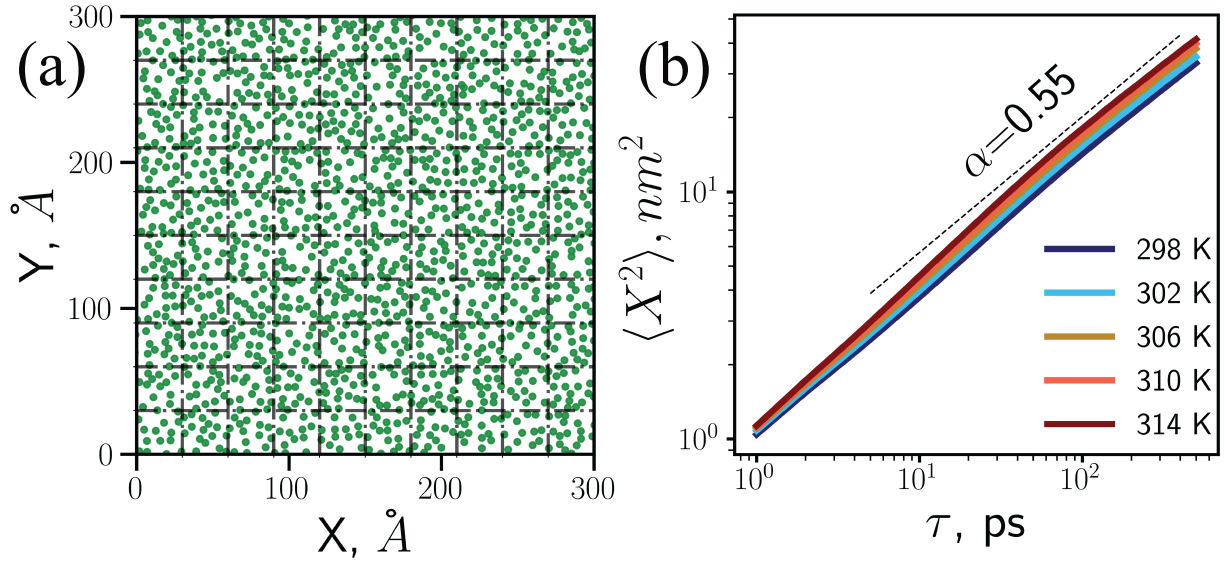


FIG. S3. Nanoscale simulation system snapshot and MSD. (a) Snapshot PO_4 groups of DPPC at 314 K (each grid = 3×3 nm). (b) MSD ($\langle X^2 \rangle$) averaged over grids at different T (298 K - 314 K).

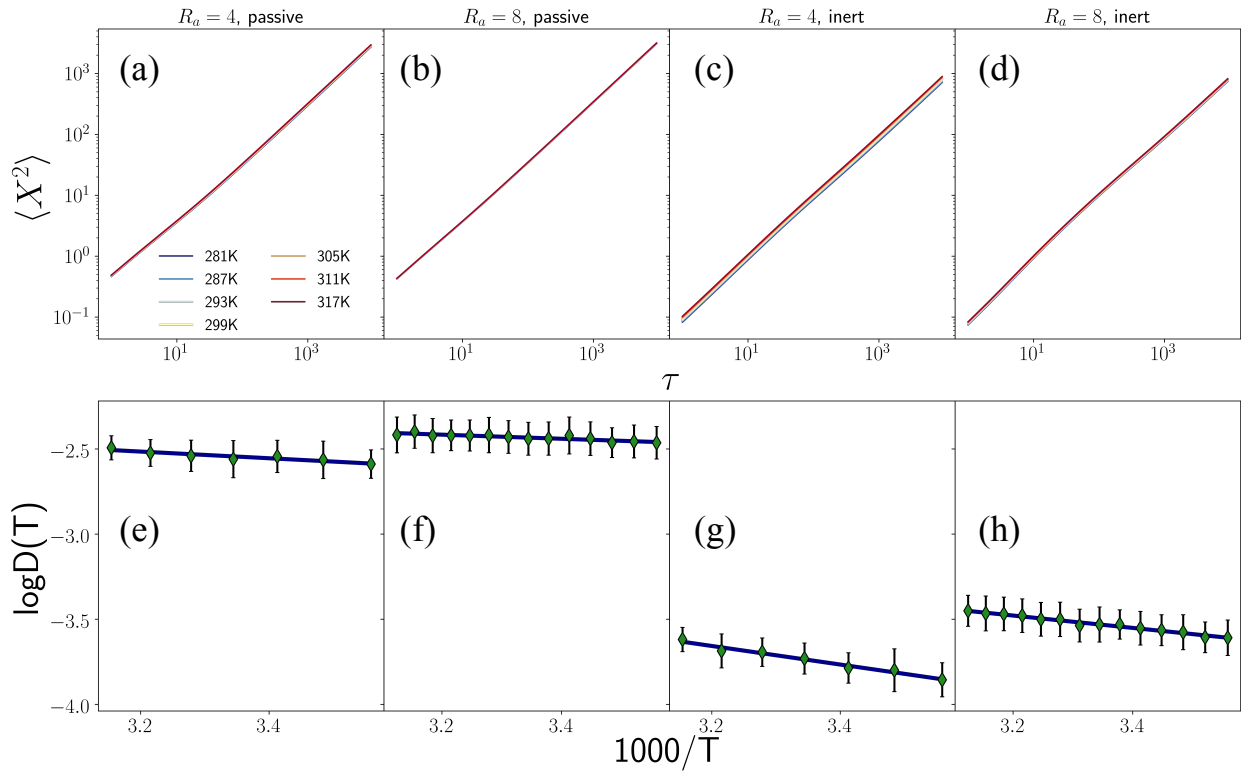


FIG. S4. Change in aster radius has no effect on diffusive behavior of lipids. The data from two different sizes of asters ($R_a = 4$ and 8) is compared in (a)-(h) for passive and inert lipids.

-
- [1] H. C. Berg and E. M. Purcell, Physics of chemoreception, *Biophysical journal* **20**, 193 (1977).
- [2] M. Javanainen, H. Martinez-Seara, R. Metzler, and I. Vattulainen, Diffusion of integral membrane proteins in protein-rich membranes, *The journal of physical chemistry letters* **8**, 4308 (2017).
- [3] B. Fábíán, I. Vattulainen, and M. Javanainen, Protein crowding and cholesterol increase cell membrane viscosity in a temperature dependent manner, *Journal of Chemical Theory and Computation* **19**, 2630 (2023).
- [4] A. Kusumi, C. Nakada, K. Ritchie, K. Murase, K. Suzuki, H. Murakoshi, R. S. Kasai, J. Kondo, and T. Fujiwara, Paradigm shift of the plasma membrane concept from the two-dimensional continuum fluid to the partitioned fluid: high-speed single-molecule tracking of membrane molecules, *Annu. Rev. Biophys. Biomol. Struct.* **34**, 351 (2005).
- [5] K. Ritchie, X.-Y. Shan, J. Kondo, K. Iwasawa, T. Fujiwara, and A. Kusumi, Detection of non-brownian diffusion in the cell membrane in single molecule tracking, *Biophysical journal* **88**, 2266 (2005).
- [6] C. Eggeling, C. Ringemann, R. Medda, G. Schwarzmann, K. Sandhoff, S. Polyakova, V. N. Belov, B. Hein, C. Von Middendorff, A. Schönle, *et al.*, Direct observation of the nanoscale dynamics of membrane lipids in a living cell, *Nature* **457**, 1159 (2009).
- [7] V. Mueller, C. Ringemann, A. Honigmann, G. Schwarzmann, R. Medda, M. Leutenegger, S. Polyakova, V. N. Belov, S. Hell, and C. Eggeling, Sted nanoscopy reveals molecular details of cholesterol-and cytoskeleton-modulated lipid interactions in living cells, *Biophysical journal* **101**, 1651 (2011).
- [8] M. J. Bowick, N. Fakhri, M. C. Marchetti, and S. Ramaswamy, Symmetry, thermodynamics, and topology in active matter, *Physical Review X* **12**, 010501 (2022).
- [9] K. Ritchie, R. Iino, T. Fujiwara, K. Murase, and A. Kusumi, The fence and picket structure of the plasma membrane of live cells as revealed by single molecule techniques, *Molecular membrane biology* **20**, 13 (2003).
- [10] Y. Oda and H. Fukuda, The dynamic interplay of plasma membrane domains and cortical microtubules in secondary cell wall patterning, *Frontiers in Plant Science* **4**, 511 (2013).

- [11] D. V. Köster and S. Mayor, Cortical actin and the plasma membrane: inextricably intertwined, [Current opinion in cell biology](#) **38**, 81 (2016).
- [12] P. Beemiller and M. F. Krummel, Regulation of t-cell receptor signaling by the actin cytoskeleton and poroelastic cytoplasm, [Immunological reviews](#) **256**, 148 (2013).
- [13] D. Goswami, K. Gowrishankar, S. Bilgrami, S. Ghosh, R. Raghupathy, R. Chadda, R. Vishwakarma, M. Rao, and S. Mayor, Nanoclusters of gpi-anchored proteins are formed by cortical actin-driven activity, [Cell](#) **135**, 1085 (2008).
- [14] F. Montalenti and R. Ferrando, Jumps and concerted moves in cu, ag, and au (110) adatom self-diffusion, [Physical Review B](#) **59**, 5881 (1999).
- [15] M. Javanainen, L. Monticelli, J. B. de la Serna, and I. Vattulainen, Free volume theory applied to lateral diffusion in langmuir monolayers: atomistic simulations for a protein-free model of lung surfactant, [Langmuir](#) **26**, 15436 (2010).
- [16] A. Debnath, K. Ayappa, and P. K. Maiti, Simulation of influence of bilayer melting on dynamics and thermodynamics of interfacial water, [Physical Review Letters](#) **110**, 018303 (2013).
- [17] N. Bag, D. H. X. Yap, and T. Wohland, Temperature dependence of diffusion in model and live cell membranes characterized by imaging fluorescence correlation spectroscopy, [Biochimica et Biophysica Acta \(BBA\)-Biomembranes](#) **1838**, 802 (2014).
- [18] S. Saha, I.-H. Lee, A. Polley, J. T. Groves, M. Rao, and S. Mayor, Diffusion of gpi-anchored proteins is influenced by the activity of dynamic cortical actin, [Molecular biology of the cell](#) **26**, 4033 (2015).
- [19] R. Macháň and M. Hof, Lipid diffusion in planar membranes investigated by fluorescence correlation spectroscopy, [Biochimica et Biophysica Acta \(BBA\)-Biomembranes](#) **1798**, 1377 (2010).
- [20] C. Favard, J. Wenger, P.-F. Lenne, and H. Rigneault, Fcs diffusion laws in two-phase lipid membranes: determination of domain mean size by experiments and monte carlo simulations, [Biophysical journal](#) **100**, 1242 (2011).
- [21] I.-H. Lee, S. Saha, A. Polley, H. Huang, S. Mayor, M. Rao, and J. T. Groves, Live cell plasma membranes do not exhibit a miscibility phase transition over a wide range of temperatures, [The Journal of Physical Chemistry B](#) **119**, 4450 (2015).
- [22] G. R. Kneller, K. Baczynski, and M. Pasenkiewicz-Gierula, Communication: Consistent picture of lateral subdiffusion in lipid bilayers: Molecular dynamics simulation and exact results,

- The Journal of chemical physics **135** (2011).
- [23] P. Macedo and T. Litovitz, On the relative roles of free volume and activation energy in the viscosity of liquids, *The Journal of Chemical Physics* **42**, 245 (1965).
- [24] W. L. Vaz, R. M. Clegg, and D. Hallmann, Translational diffusion of lipids in liquid crystalline phase phosphatidylcholine multibilayers. a comparison of experiment with theory, *Biochemistry* **24**, 781 (1985).
- [25] P. F. Almeida, W. L. Vaz, and T. Thompson, Lateral diffusion in the liquid phases of dimyristoylphosphatidylcholine/cholesterol lipid bilayers: a free volume analysis, *Biochemistry* **31**, 6739 (1992).
- [26] A. Filippov, G. Orädd, and G. Lindblom, The effect of cholesterol on the lateral diffusion of phospholipids in oriented bilayers, *Biophysical journal* **84**, 3079 (2003).
- [27] T. Apajalahti, P. Niemelä, P. N. Govindan, M. S. Miettinen, E. Salonen, S.-J. Marrink, and I. Vattulainen, Concerted diffusion of lipids in raft-like membranes, *Faraday discussions* **144**, 411 (2010).
- [28] E. Falck, T. Róg, M. Karttunen, and I. Vattulainen, Lateral diffusion in lipid membranes through collective flows, *Journal of the American Chemical Society* **130**, 44 (2008).
- [29] P. H. Poole, C. Donati, and S. C. Glotzer, Spatial correlations of particle displacements in a glass-forming liquid, *Physica A: Statistical Mechanics and its Applications* **261**, 51 (1998).
- [30] C. Bennemann, C. Donati, J. Baschnagel, and S. C. Glotzer, Growing range of correlated motion in a polymer melt on cooling towards the glass transition, *Nature* **399**, 246 (1999).
- [31] C. Donati, S. C. Glotzer, and P. H. Poole, Growing spatial correlations of particle displacements in a simulated liquid on cooling toward the glass transition, *Physical review letters* **82**, 5064 (1999).
- [32] M. D. Ediger, Spatially heterogeneous dynamics in supercooled liquids, *Annual review of physical chemistry* **51**, 99 (2000).
- [33] R. Richert, Heterogeneous dynamics in liquids: fluctuations in space and time, *Journal of Physics: Condensed Matter* **14**, R703 (2002).
- [34] T. Narumi and M. Tokuyama, Simulation study of spatial-temporal correlation functions in supercooled liquids, *Philosophical Magazine* **88**, 4169 (2008).
- [35] T. Narumi and M. Tokuyama, Study of spatial correlation functions near the glass transition by molecular dynamics simulations, *Journal of crystal growth* **311**, 707 (2009).

- [36] F. Puosi and D. Leporini, Spatial displacement correlations in polymeric systems, [The Journal of Chemical Physics](#) **136** (2012).
- [37] P. S. Pyenta, D. Holowka, and B. Baird, Cross-correlation analysis of inner-leaflet-anchored green fluorescent protein co-redistributed with ige receptors and outer leaflet lipid raft components, [Biophysical journal](#) **80**, 2120 (2001).
- [38] K. Gowrishankar, S. Ghosh, S. Saha, C. Rumamol, S. Mayor, and M. Rao, Active remodeling of cortical actin regulates spatiotemporal organization of cell surface molecules, [Cell](#) **149**, 1353 (2012).
- [39] S. Saha, A. Das, C. Patra, A. A. Anilkumar, P. Sil, S. Mayor, and M. Rao, Active emulsions in living cell membranes driven by contractile stresses and transbilayer coupling, [Proceedings of the National Academy of Sciences](#) **119**, e2123056119 (2022).
- [40] C. F. Schroer, L. Baldauf, L. van Buren, T. A. Wassenaar, M. N. Melo, G. H. Koenderink, and S. J. Marrink, Charge-dependent interactions of monomeric and filamentous actin with lipid bilayers, [Proceedings of the National Academy of Sciences](#) **117**, 5861 (2020).
- [41] A. Das, A. Polley, and M. Rao, Phase segregation of passive advective particles in an active medium, [Physical Review Letters](#) **116**, 068306 (2016).
- [42] K. Kawasaki and C. d. Domb, Phase transitions and critical phenomena (1972).
- [43] B. B. Machta, S. Papanikolaou, J. P. Sethna, and S. L. Veatch, Minimal model of plasma membrane heterogeneity requires coupling cortical actin to criticality, [Biophysical journal](#) **100**, 1668 (2011).
- [44] O. Kimchi, S. L. Veatch, and B. B. Machta, Ion channels can be allosterically regulated by membrane domains near a de-mixing critical point, [Journal of General Physiology](#) **150**, 1769 (2018).
- [45] M. Edidin and V. A. Petit, The effect of temperature on the lateral diffusion of plasma membrane proteins, in *Ciba Foundation Symposium 52-The Freezing of Mammalian Embryos*, Vol. 52 (Wiley Online Library, 1977) pp. 155–174.
- [46] Y. Wang, P. Gkeka, J. E. Fuchs, K. R. Liedl, and Z. Cournia, Dppc-cholesterol phase diagram using coarse-grained molecular dynamics simulations, [Biochimica et Biophysica Acta \(BBA\)-Biomembranes](#) **1858**, 2846 (2016).
- [47] D. Landau and K. Binder, *A guide to Monte Carlo simulations in statistical physics* (Cambridge university press, 2021).

- [48] S. Mondal, P. Popli, and S. Sarkar, Coarsening of topological defects in 2d polar active matter, [arXiv preprint arXiv:2401.00203](#) (2023).
- [49] M. Fritzsche, D. Li, H. Colin-York, V. Chang, E. Moeendarbary, J. Felce, E. Sezgin, G. Chararas, E. Betzig, and C. Eggeling, Self-organizing actin patterns shape membrane architecture but not cell mechanics, [Nature communications](#) **8**, 14347 (2017).
- [50] S. Sarkar and D. Goswami, Lifetime of actin-dependent protein nanoclusters, [Biophysical Journal](#) **122**, 290 (2023).
- [51] C. Wey, R. Cone, and M. Edidin, Lateral diffusion of rhodopsin in photoreceptor cells measured by fluorescence photobleaching and recovery, [Biophysical journal](#) **33**, 225 (1981).
- [52] H. A. Johnson and M. Pavelec, Thermal noise in cells: a cause of spontaneous loss of cell function, [The American Journal of Pathology](#) **69**, 119 (1972).
- [53] N. Barkai and S. Leibler, Robustness in simple biochemical networks, [Nature](#) **387**, 913 (1997).
- [54] M. Thattai and A. van Oudenaarden, Attenuation of noise in ultrasensitive signaling cascades, [Biophysical journal](#) **82**, 2943 (2002).
- [55] M. Thattai and A. Van Oudenaarden, Stochastic gene expression in fluctuating environments, [Genetics](#) **167**, 523 (2004).
- [56] A. Bar-Even, J. Paulsson, N. Maheshri, M. Carmi, E. O’Shea, Y. Pilpel, and N. Barkai, Noise in protein expression scales with natural protein abundance, [Nature genetics](#) **38**, 636 (2006).
- [57] J. Prost, J.-F. Joanny, and J. M. Parrondo, Generalized fluctuation-dissipation theorem for steady-state systems, [Physical review letters](#) **103**, 090601 (2009).
- [58] J. M. Horowitz and T. R. Gingrich, Thermodynamic uncertainty relations constrain non-equilibrium fluctuations, [Nature Physics](#) **16**, 15 (2020).
- [59] B. A. Bicknell, P. Dayan, and G. J. Goodhill, The limits of chemosensation vary across dimensions, [Nature communications](#) **6**, 7468 (2015).
- [60] S. Xia, Y. B. Lim, Z. Zhang, Y. Wang, S. Zhang, C. T. Lim, E. K. Yim, and P. Kanchanawong, Nanoscale architecture of the cortical actin cytoskeleton in embryonic stem cells, [Cell reports](#) **28**, 1251 (2019).
- [61] T. A. Wassenaar, H. I. Ingólfsson, R. A. Bockmann, D. P. Tieleman, and S. J. Marrink, Computational lipidomics with insane: a versatile tool for generating custom membranes for molecular simulations, [Journal of chemical theory and computation](#) **11**, 2144 (2015).

- [62] P. C. Souza, R. Alessandri, J. Barnoud, S. Thallmair, I. Faustino, F. Grünewald, I. Patmanidis, H. Abdizadeh, B. M. Bruininks, T. A. Wassenaar, *et al.*, Martini 3: a general purpose force field for coarse-grained molecular dynamics, [Nature methods](#) **18**, 382 (2021).
- [63] L. Borges-Araújo, A. C. Borges-Araújo, T. N. Ozturk, D. P. Ramirez-Echemendia, B. Fábíán, T. S. Carpenter, S. Thallmair, J. Barnoud, H. I. Ingólfsson, G. Hummer, *et al.*, Martini 3 coarse-grained force field for cholesterol, [Journal of Chemical Theory and Computation](#) **19**, 7387 (2023).
- [64] X. Lin and A. A. Gorfe, Understanding membrane domain-partitioning thermodynamics of transmembrane domains with potential of mean force calculations, [The Journal of Physical Chemistry B](#) **123**, 1009 (2019).
- [65] D. Van Der Spoel, E. Lindahl, B. Hess, G. Groenhof, A. E. Mark, and H. J. Berendsen, Gromacs: fast, flexible, and free, [Journal of computational chemistry](#) **26**, 1701 (2005).
- [66] H. Bekker, H. Berendsen, E. Dijkstra, S. Achterop, R. v. Vondrumen, D. Vanderspoel, A. Sijbers, H. Keegstra, and M. Renardus, Gromacs-a parallel computer for molecular-dynamics simulations, in *4th international conference on computational physics (PC 92)* (World Scientific Publishing, 1993) pp. 252–256.
- [67] M. J. Abraham, T. Murtola, R. Schulz, S. Páll, J. C. Smith, B. Hess, and E. Lindahl, Gromacs: High performance molecular simulations through multi-level parallelism from laptops to supercomputers, [SoftwareX](#) **1**, 19 (2015).
- [68] R. J. Gowers, M. Linke, J. Barnoud, T. J. Reddy, M. N. Melo, S. L. Seyler, J. Domanski, D. L. Dotson, S. Buchoux, I. M. Kenney, *et al.*, Mdanalysis: a python package for the rapid analysis of molecular dynamics simulations, in *Proceedings of the 15th python in science conference*, Vol. 98 (SciPy Austin, TX, 2016) p. 105.
- [69] W. Humphrey, A. Dalke, and K. Schulten, Vmd: visual molecular dynamics, [Journal of molecular graphics](#) **14**, 33 (1996).
- [70] H. I. Ingólfsson, M. N. Melo, F. J. Van Eerden, C. Arnarez, C. A. Lopez, T. A. Wassenaar, X. Periole, A. H. De Vries, D. P. Tieleman, and S. J. Marrink, Lipid organization of the plasma membrane, [Journal of the american chemical society](#) **136**, 14554 (2014).
- [71] R. M. Venable, H. I. Ingólfsson, M. G. Lerner, B. S. Perrin Jr, B. A. Camley, S. J. Marrink, F. L. Brown, and R. W. Pastor, Lipid and peptide diffusion in bilayers: The saffman–delbrück model and periodic boundary conditions, [The Journal of Physical Chemistry B](#) **121**, 3443

- (2017).
- [72] S. J. Marrink, A. H. De Vries, and A. E. Mark, Coarse grained model for semiquantitative lipid simulations, *The Journal of Physical Chemistry B* **108**, 750 (2004).
- [73] S. J. Marrink, H. J. Risselada, S. Yefimov, D. P. Tieleman, and A. H. De Vries, The martini force field: coarse grained model for biomolecular simulations, *The journal of physical chemistry B* **111**, 7812 (2007).
- [74] H. Kang and W. Weinberg, Dynamic monte carlo with a proper energy barrier: surface diffusion and two-dimensional domain ordering, *The Journal of chemical physics* **90**, 2824 (1989).
- [75] K. A. Fichthorn and W. H. Weinberg, Theoretical foundations of dynamical monte carlo simulations, *The Journal of chemical physics* **95**, 1090 (1991).
- [76] C. Uebing and R. Gomer, A monte carlo study of surface diffusion coefficients in the presence of adsorbate–adsorbate interactions. i. repulsive interactions, *The Journal of Chemical Physics* **95**, 7626 (1991).
- [77] C. Uebing and R. Gomer, Determination of surface diffusion coefficients by monte carlo methods: Comparison of fluctuation and kubo–green methods, *The Journal of chemical physics* **100**, 7759 (1994).
- [78] G. Bussi, D. Donadio, and M. Parrinello, Canonical sampling through velocity rescaling, *The Journal of chemical physics* **126** (2007).
- [79] H. J. Berendsen, J. v. Postma, W. F. Van Gunsteren, A. DiNola, and J. R. Haak, Molecular dynamics with coupling to an external bath, *The Journal of chemical physics* **81**, 3684 (1984).
- [80] S. J. Marrink and D. P. Tieleman, Perspective on the martini model, *Chemical Society Reviews* **42**, 6801 (2013).
- [81] M. Parrinello and A. Rahman, Polymorphic transitions in single crystals: A new molecular dynamics method, *Journal of Applied physics* **52**, 7182 (1981).
- [82] D. H. De Jong, S. Baoukina, H. I. Ingólfsson, and S. J. Marrink, Martini straight: Boosting performance using a shorter cutoff and gpus, *Computer Physics Communications* **199**, 1 (2016).
- [83] H. I. Ingólfsson, T. S. Carpenter, H. Bhatia, P.-T. Bremer, S. J. Marrink, and F. C. Lightstone, Computational lipidomics of the neuronal plasma membrane, *Biophysical journal* **113**, 2271 (2017).